Nanoscale

RSC Publishing

PAPER

View Article Online
View Journal | View Issue

Cite this: *Nanoscale*, 2013, **5**, 3400

Photoluminescence and time-resolved carrier dynamics in thiol-capped CdTe nanocrystals under high pressure

Yan-Cheng Lin,*[a] Wu-Ching Chou,*[a] Andrei S. Susha,[b] Stephen V. Kershaw[b] and Andrey L. Rogach[b]

Received 4th December 2012
Accepted 15th February 2013

DOI: 10.1039/c3nr33928a

www.rsc.org/nanoscale

The application of static high pressure provides a method for precisely controlling and investigating many fundamental and unique properties of semiconductor nanocrystals (NCs). This study systematically investigates the high-pressure photoluminescence (PL) and time-resolved carrier dynamics of thiol-capped CdTe NCs of different sizes, at different concentrations, and in various stress environments. The zincblende-to-rocksalt phase transition in thiol-capped CdTe NCs is observed at a pressure far in excess of the bulk phase transition pressure. Additionally, the process of transformation depends strongly on NC size, and the phase transition pressure increases with NC size. These peculiar phenomena are attributed to the distinctive bonding of thiols to the NC surface. In a nonhydrostatic environment, considerable flattening of the PL energy of CdTe NC powder is observed above 3.0 GPa. Furthermore, asymmetric and double-peak PL emissions are obtained from a concentrated solution of CdTe NCs under hydrostatic pressure, implying the feasibility of pressure-induced interparticle coupling.

Introduction

Semiconductor nanocrystals (NCs), commonly referred to as colloidal quantum dots (QDs), hold immense promise for use in optoelectronic, biological, and medical applications because of their unique optical properties, including size-tunable photoluminescence (PL), high PL quantum yield (QY), narrow emission bandwidth, broad absorption profile, superior photostability, and flexible solution processing.[1–5] Owing to the large surface-to-volume ratio of NCs, the state of the surface critically affects many of their properties. Synthesis in organic solvents using long-chain trioctylphosphine (TOP)/trioctylphosphine oxide (TOPO) ligands is one of the most mature methods for preparing highly fluorescent II–VI NCs that are insoluble in water.[6–8] The hydrophobic NCs must be transferred into the aqueous phase *via* ligand exchange, which is a prerequisite for applications in biomedicine.[9,10] However, this process generally reduces the photostability, solubility in water, and PL QY drastically because of the strong polarity of water molecules. Hence, the direct aqueous synthesis of semiconductor NCs with high PL QY has become a rich field of scientific endeavor.

Water-soluble thiol-capped CdTe NCs have been demonstrated to be the most robust and highly fluorescent nanoparticles that can be directly synthesized in aqueous solution.[11–14] The use of short-chain thiols, such as thioglycolic acid (TGA) and mercaptopropionic acid (MPA), favors control of the kinetics of the NC synthesis, passivation of the surface dangling bonds, and extension of the surface functionality to various hybrid structures.[15–18] Although the fundamental properties of thiol-capped CdTe NCs and their wide range of applications that use Förster resonance energy transfer (FRET) have been extensively studied under ambient pressure,[15,19,20] whether the short-chain thiols influence the photostability, crystalline stability, phase transition, and carrier dynamics of water-soluble CdTe NCs under high pressure remains unexplored. High pressure changes the surface states, structural phases and electronic properties of NCs, as well as the spacing between adjacent particles, modulating nearest-neighbor and long-range interactions. Alivisatos and Tolbert performed pioneering high-pressure research on semiconductor NCs to study the effect of finite size on the solid–solid phase transformation of CdSe NCs.[21] The phase transition from wurtzite to rocksalt in CdSe NCs is strongly size dependent unlike the corresponding bulk material, occurs several GPa higher, and is highly hysteretic. Yuan *et al.*[22] and Fan *et al.*[23] investigated the electronic and vibrational states of CdSe/ZnS core/shell NCs under high pressure and found that the ZnS shell dominates the electronic state and structural stability of such a system. While recently examining CdSe QD solids at an elevated pressure, Grant *et al.* demonstrated that the pressure medium significantly affects the dependence of the PL emission on pressure.[24]

This study comprehensively investigated the electronic states, crystalline stability, and carrier decay dynamics of water-soluble thiol-capped CdTe NCs using high-pressure PL and

[a]*Department of Electrophysics, National Chiao Tung University, Hsinchu 30010, Taiwan. E-mail: bryanlin@mail.nctu.edu.tw; wuchingchou@mail.nctu.edu.tw*

[b]*Department of Physics and Materials Science and Centre for Functional Photonics (CFP), City University of Hong Kong, Hong Kong SAR*

time-resolved PL (TRPL) spectroscopy. The bonding of the stabilizer thiols to the NC surface determines the phase transition pressure and the dependence of the emission energy on pressure. To study thoroughly the surface effects, high-pressure measurements of thiol-capped CdTe NCs of different sizes, at different concentrations, and in various stress environments are carefully made. The optical and electronic properties of NCs are strongly related to their crystalline stability and surface conditions. Accordingly, understanding the effects of the surface on the phase transition and carrier decay dynamics at the nanoscale would facilitate the development of nanomaterials and devices.

Experimental section

Highly luminescent CdTe NCs were directly synthesized in aqueous solution, following a procedure that has been published previously.[13] The water-soluble CdTe NCs that were used in this study were surface-stabilized by applying 3-mercaptopropionic acid (MPA). The sizes of the MPA-capped CdTe NCs with diameters of d = 2.3, 3.4, and 5.1 nm were determined according to the sizing curve that was obtained by Rogach *et al.* by both transmission electron microscopy (TEM) and powder X-ray diffraction (XRD) analyses.[13] The MPA-capped CdTe NCs exhibited a narrow size distribution of ~5% and were highly crystalline with a zincblende (ZB) structure under ambient conditions. Room-temperature absorption spectra were recorded in air using a Cary 50 spectrometer (Varian). High-pressure PL and TRPL measurements were all made at room temperature using a ruby-calibrated diamond anvil cell (DAC).[25] The pressure-transmitting medium was Milli-Q water (Millipore), and the pressure gradient was less than 0.2 GPa throughout the sample chamber. The PL and TRPL of the CdTe NCs and the ruby fluorescence were excited using a 200 ps pulsed laser diode (405 nm/2.5 MHz/1 mW), which was focused onto the sample using a 20× Olympus objective with a long working distance. Signals were dispersed using a Horiba iHR550 spectrometer with a 1800 gr/mm grating and detected using a multichannel LN_2-cooled charge-coupled device (CCD) and a photon-counting avalanche photodiode. The decay traces were recorded by time-correlated single photon counting (Time-Harp, PicoQuant).

Results and discussion

Fig. 1 shows the absorption and PL spectra of MPA-capped CdTe NCs (d = 2.3, 3.4, and 5.1 nm) in aqueous solution under ambient conditions. The CdTe NCs provide blue, red, and near-infrared emissions, centered at 530, 615, and 720 nm, respectively. At ambient pressure, a slight Stokes shift of the emission peaks relative to the excitonic absorption peaks is observed, revealing that the near-band-edge emissions, rather than the deep traps dominate the PL of MPA-capped CdTe NCs. The NC concentrations are all fixed at 250 nM, such that the interactions between the adjacent NCs of slightly different sizes within the entire ensemble are negligible, on which high-pressure research on NCs with short-chain surface ligands depends.

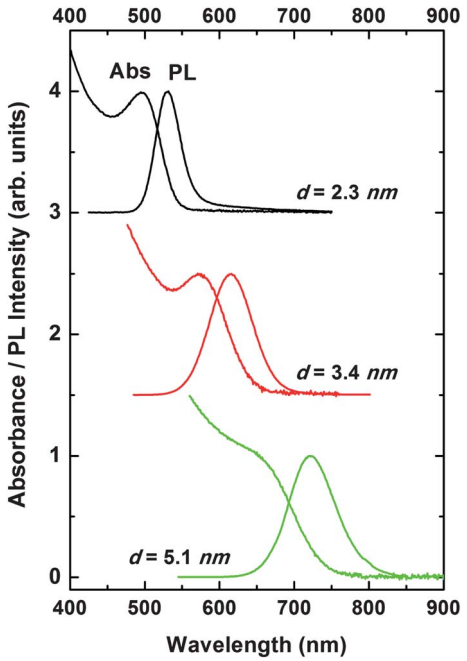

Fig. 1 Absorption and PL spectra of aqueous (250 nM) MPA-capped CdTe NCs under ambient pressure.

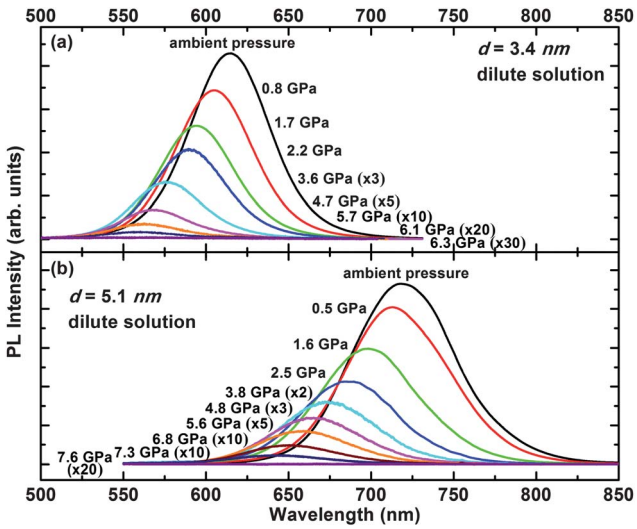

Fig. 2 Pressure-dependent PL spectra of aqueous (250 nM) (a) 3.4 nm and (b) 5.1 nm MPA-capped CdTe NCs.

Fig. 2(a) shows the pressure-dependent PL spectra of aqueous CdTe NCs (d = 3.4 nm; 250 nM) that are recorded under increasing pressure up to 6.3 GPa. As the external pressure is applied, the PL peaks shift monotonically toward lower wavelength. These shifts are accompanied by significant falls in emission intensities. The large PL energy blueshift of the NCs is caused by the pressure-induced reduction in lattice constants. When the pressure is slowly increased to a critical value of around 6.3 GPa, the PL emission of CdTe NCs suddenly disappears and the sample darkens. The above phenomena at high pressure are strong evidence of the pressure-induced metallization of CdTe NCs.[22,23] This tendency of transformation was

first identified in a high-pressure resistivity study of bulk CdTe crystals, whose resistivity abruptly drops over three orders of magnitude at around 3.8 GPa.[26] Additionally, XRD measurements of CdTe bulk indicate that the phase transformation from a fourfold-coordinated ZB to a sixfold-coordinated rocksalt (RS) structure is complete at around 3.8 GPa with a 16% reduction in volume.[27] This finding demonstrates that the pressure-induced metallization of CdTe occurs when the crystalline phase transforms from ZB to RS. Obviously, the ZB-to-RS transition pressure of 3.4 nm CdTe NCs (6.3 GPa) exceeds that of the bulk CdTe (3.8 GPa). Similar experimental results have also been obtained for CdSe NCs, in which the wurtzite (WZ) phase of CdSe NCs is stable under pressures that are two to three times above that at which the bulk is stable (2.0 GPa), depending on the size of the NCs.[21] The transition pressure of the NCs is higher than that of the bulk because of the surface energy effects. The phase transition pressure can be obtained by a common-tangent construction between the energy–volume curves of the two phases ($P_T = -dU/dV$).[21] Restated, the changes in transition pressure can be determined from differences between the surface energies of the two phases. Although the surface energy raises the energy of the ZB(WZ) phase NCs relative to the ZB(WZ) bulk, it increases the energy of the RS phase NCs even more relative to that of the RS phase bulk. Accordingly, the slope of the common-tangent line (phase transition pressure) is higher for NCs.

Fig. 2(b) shows the up-stroke pressure-dependent PL spectra of large CdTe NCs ($d = 5.1$ nm; 250 nM). The pressure-induced emission wavelength shifts are accompanied by significant declines in emission intensities. As can be seen in Fig. 2(b), the PL emission band is still observable above 6.3 GPa upon compression. The emission band gradually vanishes upon further compression and completely disappears by 7.6 GPa. Also, the sample in the DAC abruptly changes from bright to dark. Restated, the ZB-to-RS phase transition of 5.1 nm CdTe NCs is complete at around 7.6 GPa, which value is higher than that of 3.4 nm CdTe NCs. However, close inspection of the transition of small CdTe NCs (2.3 nm; 250 nM) reveals that the ZB-to-RS phase transition is complete earlier than that of large CdTe NCs (3.4 and 5.1 nm). Table 1 summarizes the obtained ZB-to-RS phase transition pressures for all of the MPA-capped CdTe NCs. Clearly, the phase transition pressures increase with NC size. This behavior is in contrast to that of the 4-ethyl-pyridine capped CdSe NCs, whose phase transition pressure increases as the NC size decreases.[21] The difference between MPA-capped CdTe and the CdSe NCs with this weakly bound capping agent is attributable to their distinctly different surface conditions.

Table 1 Phase transition pressures, quadratic pressure coefficients $dE(P)/dp$, and energy shifts (ΔE) at phase transition pressures for aqueous (250 nM) MPA-capped CdTe NCs

NC size in diameter (nm)	Phase transition pressure (GPa)	$dE(P)/dp$ (meV/GPa)	ΔE (meV)
2.3	5.8 ± 0.2	53.0–6.0p	206.5 ± 3.8
3.4	6.3 ± 0.2	46.0–4.2p	206.5 ± 4.0
5.1	7.6 ± 0.2	36.5–2.6p	202.3 ± 3.5

The pressure-induced phase transitions typically nucleate on NC surface defects and proceed inward as the pressure is increased.[28] Therefore, the surface control of NCs is crucial not only to photostability and PL QY, but also to crystalline stability. Heteroepitaxially growing an inorganic shell of a wider band-gap semiconductor on the surface of NCs, such as CdSe/ZnS core–shell NCs, whose shell acts as a barrier as well as a protector for the core, improves the luminescence efficiency and increases the phase transition pressure.[22,23] In the case of CdTe NCs with thiol as the surface stabilizer, discussed herein, the thiols with a polar headgroup passivate surface dangling bonds and making NCs water-soluble. Although an inorganic shell is not grown intentionally, an ultra-thin sulfur-capped surface (CdS shell) is formed naturally because mercapto-groups are covalently attached to the surface cadmium atoms.[13,29] CdS is an excellent shell material for CdTe cores not only because its band gap (2.5 eV) is larger than that of CdTe (1.5 eV) but also because its lattice mismatch with CdTe (10.1%) is smaller than that of ZnSe (12.5%) and ZnS (16.5%).[30] Moreover, the bulk modulus of the CdS (62.0 GPa) exceeds that of CdTe (42.0 GPa).[31,32] Thus, the CdS shell acts as a gentle protector of the CdTe core. Earlier experimental results reveal that the increase in the amount of MPA(TGA) in solution at the synthesis stage and prolonged heating of NC suspensions considerably increase the probability of stabilizer hydrolysis, resulting in a higher sulfur content in the NCs.[13] Consequently, longer synthesis corresponds to larger CdTe NCs that are covered with thicker CdS surface shells. These facts explain the peculiar size-dependence of the ZB-to-RS phase transition pressures of MPA-capped CdTe NCs.

Fig. 3 plots the pressure-induced PL peak energy shifts of all of the CdTe NCs. The solid lines are the least-squares fit to the experimental data using a quadratic equation, $E_{PL}(P) = E_0 + \alpha P + \beta P^2$, where $E_{PL}(P)$ is the PL peak energy in eV, E_0 is the PL peak energy at ambient pressure, α is the initial linear slope of the curve and is closely related to the bulk modulus (the reciprocal of the isothermal compressibility) under ambient

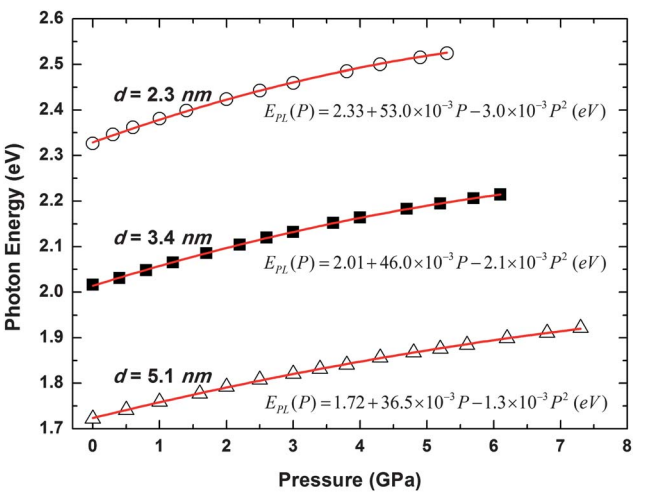

Fig. 3 Pressure-dependence of observed PL peak energies of aqueous (250 nM) MPA-capped CdTe NCs. Solid lines are quadratic polynomial fits to experimental data.

conditions, β is the nonlinear factor which indicates a variable bulk modulus under pressure, and P is the applied pressure in GPa. Thus, the pressure-induced PL peak energy shifts directly reflect the pressure-dependent lattice compressibilities of the CdTe NCs. The pressure coefficients derived from the fits to experimental data are displayed in Fig. 3 and summarized in Table 1. Several conclusions can be drawn. (i) None of the energy–pressure curves could be fitted linearly. (ii) The slopes of all the curves decrease as the applied pressure increases. (iii) As the NC size increases, the pressure coefficient α declines rapidly. (iv) The energy shifts (ΔE) for all the CdTe NCs at the critical pressure of the phase transition are almost equal. The above findings imply that the nonlinear factors greatly influence the relationship between PL peak energy and pressure. Owing to the volume change under applied pressure, the bulk modulus is not a constant but increases with increasing pressure. This trend reflects the fact that the NCs become more difficult to compress under higher pressures; consequently, the slopes decline. Additionally, the decline in α with an increase in the size of the NCs indicates that the thiol-capped CdTe NCs with thick CdS surface capping have a larger bulk modulus than the small NCs. The energy shifts of all the CdTe NCs within the ZB phase before the phase transformation are similar, implying that the relative reduction of the unit cell volume in the NCs is the same, regardless of the size before any transformation.

The PL emission peaks and linewidths of the aqueous (250 nM) MPA-capped CdTe NCs shift smoothly and symmetrically with pressure, as shown in Fig. 2 and 3. However, previous experimental results concerning CdSe QD solids at high pressure show that, depending on the pressure medium, the PL energies either increase regularly as a function of pressure or, after an initial increase, they flatten or even decrease with pressure.[24] Asymmetric and double-peak PL emission profiles were also observed. Grant *et al.* demonstrated that the anomalous PL behavior is caused by nonhydrostatic stresses, but they did not definitively assign a mechanism of the asymmetric and double-peak PL emission.[24] To verify the dependence of nonuniform stress on the PL emissions, high-pressure PL measurements were made in a nonhydrostatic environment. Fig. 4(a) shows the pressure-dependent PL spectra of the CdTe NC powder (d = 3.4 nm) that was directly compressed in the absence of a pressure medium. At ambient pressure, the PL peak at 635 nm (1.95 eV) exhibits a pronounced energy redshift from that in aqueous solution [Fig. 2(a)]. The energy redshift in CdTe NC powder is caused by the FRET between adjacent NCs of slightly different sizes in the ensemble.[20] As the pressure increases, the emission wavelength passes through a minimum of 585 nm (2.12 eV) at around 4.7 GPa, and then remains unchanged as the pressure is increased to 6.1 GPa. The flattening of the PL peak energy of the CdTe NC powder results from the shearing effects of nonhydrostatic compression.[24] Notably, in Fig. 4(a), the PL emission vanishes at around 6.3 GPa, which is exactly the same phase transition pressure as that of aqueous (250 nM) 3.4 nm CdTe NCs. However, the asymmetric and double-peak PL behavior is not observed in CdTe NC powder under a nonuniform environment.

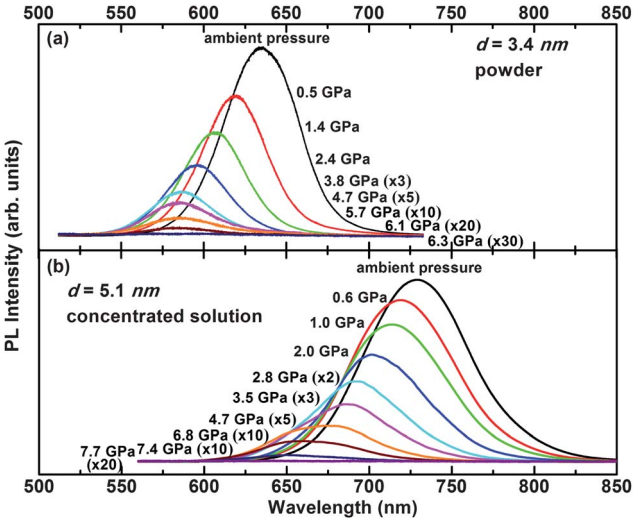

Fig. 4 Pressure-dependent PL spectra of (a) 3.4 nm MPA-capped CdTe NC powder and (b) aqueous (1.0 M) 5.1 nm MPA-capped CdTe NCs.

Fig. 4(b) shows the pressure-dependent PL spectra of aqueous CdTe NCs (d = 5.1 nm; 1.0 M). Similarly to aqueous (250 nM) 5.1 nm CdTe NCs, under hydrostatic conditions, the PL peaks shift monotonically toward lower wavelength, with falling emission intensities. The ZB-to-RS phase transition is complete by around 7.7 GPa, which value is close to that obtained for dilute CdTe NCs (d = 5.1 nm; 250 nM). However, in contrast to the results obtained for dilute CdTe NCs, an asymmetric and double-peak feature start to appear, especially at pressures of over 3.5 GPa. These phenomena, which occur only under high pressures, are also observed in CdTe NCs of various sizes and become even more pronounced for small NCs. This behavior is very likely to be caused by the transfer of energy by the pressure-induced reduction of interparticle separation. To confirm the potential effect of energy transfer in concentrated solutions of CdTe NCs at high pressure, high-pressure TRPL measurements were made.

Fig. 5(a) and (b) and 6(a) and (b) show the pressure-dependent TRPL spectra of aqueous CdTe NCs (d = 5.1 nm; 1.0 M) monitored at 630, 660, 720, and 750 nm, respectively. The insets in Fig. 5 and 6 summarize the dependence of intensity averaged PL decay lifetimes (τ_{avg}) as a function of pressure. In Fig. 5(a), as the external pressure increases, the overall PL decay lifetime sharply decreases. Additionally, the rapid decay within the initial few ns after excitation becomes pronounced as pressure increases. These experimental findings can be understood as follows. Even though the TRPL spectra are all obtained at 630 nm, the PL emissions are generated by NCs under very different conditions. For example, the PL emission at 630 nm under ambient pressure is generated primarily by a particular size fraction of the NCs. However, the emission at 630 nm under 3.5 GPa is from larger, compressed NCs, whose electronic structure is altered by the externally applied pressure. Therefore, changes in crystal structure, surface condition, and NC size decrease the PL decay lifetime. Reducing the CdTe NC size caused the traps that originated from the Te surface atoms to move from outside to inside the band gap of CdTe NCs, causing the initial fast decay.[13]

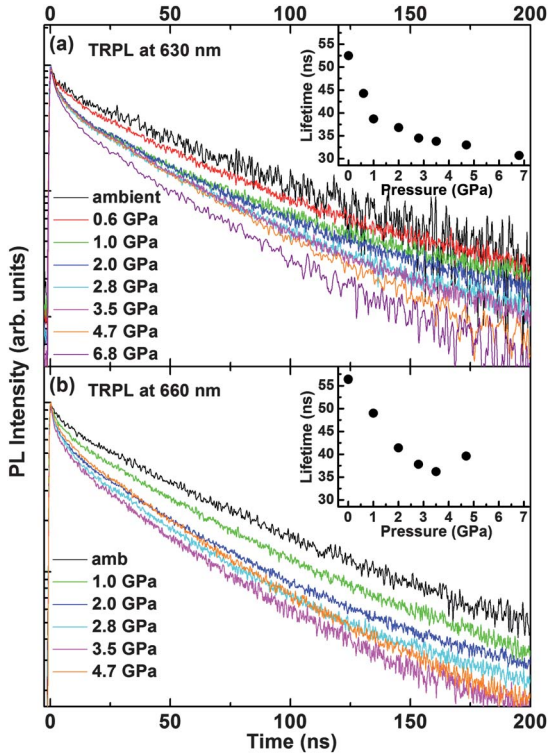

Fig. 5 Pressure-dependent TRPL spectra of aqueous (1.0 M) 5.1 nm MPA-capped CdTe NCs at (a) 630 nm and (b) 660 nm. The insets show the pressure-dependent average PL decay lifetimes (τ_{avg}).

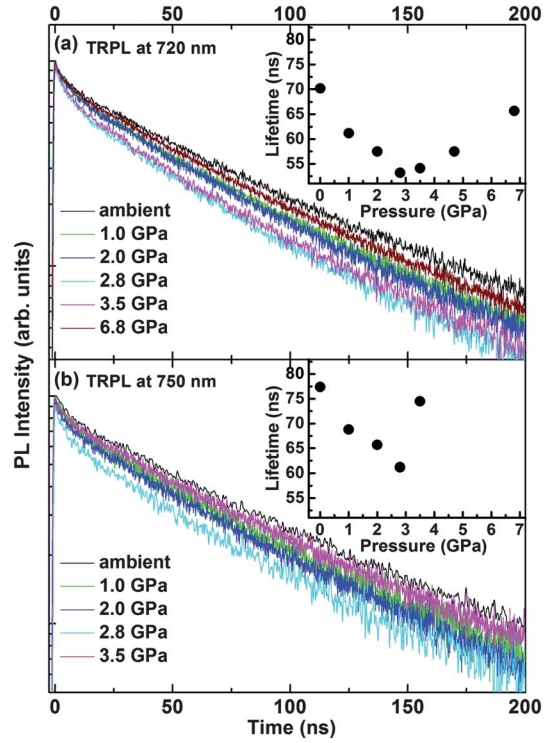

Fig. 6 Pressure-dependent TRPL spectra of aqueous (1.0 M) 5.1 nm MPA-capped CdTe NCs at (a) 720 nm and (b) 750 nm. The insets show the pressure-dependent average PL decay lifetimes (τ_{avg}).

Although the external pressure causes a significant shift in the emission wavelength, the TRPL spectra that are recorded at 630 nm over the entire range of pressures reflect mostly the decay dynamics of relatively small NCs. When the detecting wavelength is increased to 660 nm [Fig. 5(b)], an increase in average PL decay lifetime is observed above 3.5 GPa, where the detection energy approaches the PL peak. To gain insight into the decay dynamics of concentrated solutions of CdTe NCs, the detecting position is shifted toward longer wavelengths. As can be seen in Fig. 6(a), the average PL decay lifetime initially declines with increasing pressure up to 2.8 GPa and then monotonically increases with further compression, yielding a relatively narrow decay lifetime distribution. These effects are even stronger in the long-wavelength emissions, as presented in Fig. 6(b), in which the decay dynamics, recorded at 750 nm, are mostly from the relatively large NCs. However, in dilute CdTe NCs, only a monotonic, slow, and wavelength-independent reduction of the overall PL decay lifetime is observed. The above TRPL results provide clear evidence of pressure-driven nonradiative energy transfer from donors (small NCs) to acceptors (large NCs),[15,19,20] which is responsible for the asymmetric and double-peak PL emissions in concentrated solutions of CdTe NCs at high pressures. This behavior is not exhibited by CdTe NC powder in the absence of a pressure medium [Fig. 4(a)] because the NCs are already closely packed in a dry powder, and the nonradiative energy transfer between the nearest-neighbor NCs leads to the PL peak energy redshift under ambient pressure already.

Conclusions

This study investigated the emission properties, crystalline stability, and carrier decay dynamics in water-soluble MPA-capped CdTe NCs under high pressure using PL and TRPL spectroscopy. The ZB-to-RS phase transition pressure of the CdTe NCs increases as the NC size increases. As the NC size increases from 2.3 to 5.1 nm, the transformation pressure increases from 5.8 to 7.6 GPa. However, the slope of the pressure-dependent PL peak energy falls as the NC size increases. These experimental findings are attributed to the protection that is provided by the CdS surface that forms naturally owing to the stabilizer thiols, whose thickness is governed by the duration of NC growth. Additionally, the anomalous pressure-dependent PL behavior, a flattening or even a decrease in the PL energy above 3 GPa, is caused by the nonhydrostatic compression. However, pressure-induced nonradiative energy transfer from small to large NCs in concentrated NC solution, confirmed by high-pressure TRPL measurements, leads to asymmetric and double-peak PL emissions under high pressure. These effects must be considered in any investigation of pressure-mediated phenomena.

Acknowledgements

This work was supported by the Ministry of Education and the National Science Council under grant no. NSC 101-2119-M-009-001-MY2, and by a grant from the Research Grants Council of the Hong Kong S.A.R., China (project CityU 102412).

References

1 V. L. Colvin, M. C. Schlamp and A. P. Alivisatos, *Nature*, 1994, **370**, 354–357.
2 A. P. Alivisatos, *Science*, 1996, **271**, 933–937.
3 M. J. Bruchez, M. Moronne, P. Gin, S. Weiss and A. P. Alivisatos, *Science*, 1998, **281**, 2013–2016.
4 W. C. W. Chan and S. Nie, *Science*, 1998, **281**, 2016–2018.
5 A. L. Rogach, *Semiconductor Nanocrystal Quantum Dots*, Springer, Wien, 2008.
6 C. B. Murray, D. J. Norris and M. G. Bawendi, *J. Am. Chem. Soc.*, 1993, **115**, 8706–8715.
7 X. Peng, M. C. Schlamp, A. V. Kadavanich and A. P. Alivisatos, *J. Am. Chem. Soc.*, 1997, **119**, 7019–7029.
8 Z. A. Peng and X. Peng, *J. Am. Chem. Soc.*, 2001, **123**, 183–184.
9 J. K. Jaiswal, H. Mattoussi, J. M. Mauro and S. M. Simon, *Nat. Biotechnol.*, 2003, **21**, 47–51.
10 S. Kim and M. G. Bawendi, *J. Am. Chem. Soc.*, 2003, **125**, 14652–14653.
11 A. L. Rogach, L. Katsikas, A. Kornowski, D. Su, A. Eychmüller and H. Weller, *Ber. Bunsen-Ges. Phys. Chem.*, 1996, **100**, 1772–1778.
12 N. Gaponik, D. V. Talapin, A. L. Rogach, K. Hoppe, E. V. Shevchenko, A. Kornowski, A. Eychmüller and H. Weller, *J. Phys. Chem. B*, 2002, **106**, 7177–7185.
13 A. L. Rogach, T. Franzl, T. A. Klar, J. Feldmann, N. Gaponik, V. Lesnyak, A. Shavel, A. Eychmüller, Y. P. Rakovich and J. F. Donegan, *J. Phys. Chem. C*, 2007, **111**, 14628–14637.
14 N. Gaponik and A. L. Rogach, *Phys. Chem. Chem. Phys.*, 2010, **12**, 8685–8693.
15 A. L. Rogach, *Nano Today*, 2011, **6**, 355–365.
16 M. Lunz, V. A. Gerard, Y. K. Gun'ko, V. Lesnyak, N. Gaponik, A. S. Susha, A. L. Rogach and A. L. Bradley, *Nano Lett.*, 2011, **11**, 3341–3345.
17 H. Yang, W. Fan, A. Vaneski, A. S. Susha, W. Y. Teoh and A. L. Rogach, *Adv. Funct. Mater.*, 2012, **22**, 2821–2829.
18 N. Yaacobi-Gross, N. Garphunkin, O. Solomeshch, A. Vaneski, A. S. Susha, A. L. Rogach and N. Tessler, *ACS Nano*, 2012, **6**, 3128–3133.
19 A. L. Rogach, T. A. Klar, J. M. Lupton, A. Meijerink and J. Feldmann, *J. Mater. Chem.*, 2009, **19**, 1208–1221.
20 Y. C. Lin, W. J. Wang, H. L. Chung, W. C. Chou, W. K. Chen, W. H. Chang, A. S. Susha and A. L. Rogach, *Appl. Phys. Lett.*, 2009, **95**, 133123.
21 S. H. Tolbert and A. P. Alivisatos, *Science*, 1994, **265**, 373–376.
22 C. T. Yuan, Y. C. Lin, Y. N. Chen, Q. L. Chiu, W. C. Chou, D. S. Chuu, W. H. Chang, H. S. Lin, R. C. Ruaan and C. M. Lin, *Nanotechnology*, 2007, **18**, 185402.
23 H. M. Fan, Z. H. Ni, Y. P. Feng, X. F. Fan, J. L. Kuo, Z. X. Shen and B. S. Zou, *Appl. Phys. Lett.*, 2007, **90**, 021921.
24 C. D. Grant, J. C. Crowhurst, S. Hamel, A. J. Williamson and N. Zaitseva, *Small*, 2008, **4**, 788–794.
25 Y. C. Lin, C. L. Tseng, W. C. Chou, C. H. Chia, T. C. Han and J. L. Shen, *J. Phys. Chem. C*, 2011, **115**, 19962–19970.
26 C. He, C. X. Gao, B. G. Liu, M. Li, X. W. Huang, A. M. Hao, C. L. Yu, D. M. Zhang, Y. Wang, H. W. Liu, Y. Z. Ma and G. T. Zou, *J. Phys.: Condens. Matter*, 2007, **19**, 425223.
27 M. I. McMahon, R. J. Nelmes, N. G. Wright and D. R. Allan, *Phys. Rev. B: Condens. Matter*, 1993, **48**, 16246–16251.
28 C. C. Chen, A. B. Herhold, C. S. Johnson and A. P. Alivisatos, *Science*, 1997, **276**, 398–401.
29 J. Rockenberger, L. Tröger, A. L. Rogach, M. Tischer, M. Grundmann, A. Eychmüller and H. Weller, *J. Chem. Phys.*, 1998, **108**, 7807–7815.
30 T. Trindade, P. O. Brien and N. L. Pickett, *Chem. Mater.*, 2001, **13**, 3843–3858.
31 M. Haase and A. P. Alivisatos, *J. Phys. Chem.*, 1992, **96**, 6756–6762.
32 K. Strössner, S. Ves, W. Dieterich, W. Gebhardt and M. Cardona, *Solid State Commun.*, 1985, **56**, 563–565.